Biomass Gasification in Supercritical Water†

Michael Jerry Antal, Jr.,* Stephen Glen Allen, Deborah Schulman, and Xiaodong Xu

Hawaii Natural Energy Institute, University of Hawaii at Manoa, Honolulu, Hawaii 96822

Robert J. Divilio

Combustion Systems Inc., Silver Spring, Maryland 20901-2711

Biomass feedstocks, including corn- and potato-starch gels, wood sawdust suspended in a cornstarch gel, and potato wastes, were delivered to three different tubular flow reactors by means of a "cement" pump. When rapidly heated to temperatures above 650 °C at pressures above the critical pressure of water (22 MPa), the organic content of these feedstocks vaporized. A packed bed of carbon within the reactor catalyzed the gasification of these organic vapors in the water; consequently, the water effluent of the reactor was clean. The gas was composed of hydrogen, carbon dioxide, methane, carbon monoxide, and traces of ethane. Its composition was strongly influenced by the peak temperature of the reactor and the condition of the reactor's wall. Extraordinary yields (>2 L/g) of gas with a high content of hydrogen (57 mol %) were realized at the highest temperatures employed in this work. Irrespective of the reactor geometry and method of heating, all three reactors plugged after 1−2 h of use with feedstocks that contained 15 wt % organic material. Lower loadings of organics lengthened the time before plugging occurred. The plug resulted from accumulations of ash and small amounts of char formed by coking reactions involving the biomass vapors. A method for removing plugs from the reactor was developed and employed during an 8-h gasification run involving potato wastes. Extensive corrosion of each reactor's inner wall occurred during these tests. Nickel and other metals were leached from the reactor and deposited in the carbon catalyst. Nickel alloy tubes are not suitable for use in this application.

Introduction

Current enthusiasm for the use of hydrogen as an alternative transportation fuel is founded on the expectation that the hydrogen will be produced from renewable resources at a competitive price. One method of achieving this goal is the steam reforming of biomass.[1,2]

$$C_6H_{10}O_5 + 7H_2O \rightarrow 6CO_2 + 12H_2 \qquad (1)$$

In this idealized, stoichiometric equation, cellulose (represented as $C_6H_{10}O_5$) reacts with water to produce hydrogen and carbon dioxide, mimicking the commercial manufacture of hydrogen from methane by catalytic steam-reforming chemistry.[3−6] More realistically, a practical technology must convert the cellulose, hemicellulose, lignin, protein, and extractive components of the biomass feedstock to a gas rich in hydrogen and carbon dioxide, but also including some methane and carbon monoxide. Unfortunately, biomass does not react directly with steam to produce the desired products. Instead, significant amounts of tar and char are formed, and the gas contains higher hydrocarbons in addition to the desired light gases.[2,7−10] The recent work of Corella and co-workers[11] nicely illustrates the situation. In a fluid bed operating at atmospheric pressure, Corella's group observed yields of char from the steam gasification of wood sawdust in the range of 20−10 wt % and yields of tar decreasing to 4 wt % as the temperature of the bed increased from 650 to 775 °C. At the highest temperature, however, only 80% of the carbon in the feedstock was converted to gas. By employing a secondary, fluidized bed of calcined dolomite operating at 800−875 °C, Corella and co-workers[12] were able to convert almost all of the tar to gas. Nevertheless, the char byproduct was not converted and represents an effective loss of gas. Many other workers have reported similar results.[13] Thus, the formation of pyrolytic char and tar during gasification limits our ability to steam reform biomass.

An important breakthrough occurred in 1985, when Modell[14] described experiments involving the quick immersion of maple wood sawdust in supercritical water. The sawdust quickly decomposed to tars and some gas in the supercritical water without the formation of char. The explanation for this unexpected result lies in measurements of the pyrolysis kinetics of biomass materials. Cellulose is stable at higher temperatures than either hemicellulose or lignin;[15] nevertheless, cellulose decomposes rapidly at temperatures below the critical temperature of water.[16,17] Thus, Modell's experiments involved pyrolysis of wood sawdust in *liquid* water (i.e., the water nearby and within the wood sawdust was at subcritical temperatures during pyrolysis). The reactions of biomass and its components in liquid water have been a focus of much interest in the research community. At temperatures above 190 °C, the

* Author to whom correspondence should be addressed. Phone: 808/956-7267. Fax: 808/956-2336. E-mail: antal@wiliki.eng.hawaii.edu.

† We dedicate this paper to Dr. Robert H. Williams in celebration of his 25 years as Head of the Energy Technology Assessment/Energy Policy Analysis Group of the Center for Energy and Environmental Studies with Princeton University.

10.1021/ie0003436 CCC: $19.00
Published on Web 10/14/2000

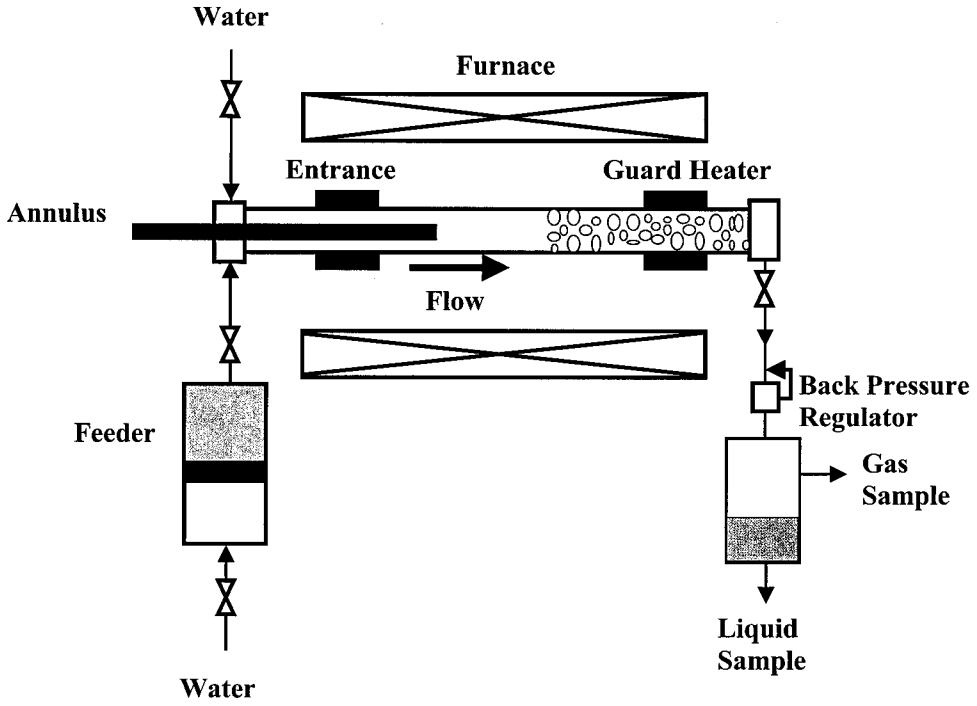

Figure 1. Schematic diagram of reactor #1. HPLC pumps and external cooling water jackets not shown.

lignin and hemicellulose macromolecules undergo solvolysis after only a few minutes of exposure to hot liquid water.[18−23] For example, after only 2 min at 220 °C, all of the hemicellulose and much of the lignin dissolves in hot liquid water.[21] Hydrothermolysis of the remaining lignocellulosic solid occurs at somewhat higher temperatures. The initial products of these solvolysis reactions subsequently undergo an extraordinary variety of isomerization, dehydration, fragmentation, and condensation reactions[24−33] that ultimately form gas and tars.[34,35] At temperatures above 600 °C and pressures in excess of the critical pressure, the primary product of the hydrothermolysis chemistry is a combustible gas composed of hydrogen, methane, carbon dioxide, and carbon monoxide, together with some tar.[36−38]

As evidenced in the work of Corella and his colleagues[11] discussed above, temperatures in excess of 700 °C effectively convert most (but not all) of the tars to gas.[2,8,10] Much work has been reported on the use of heterogeneous catalysts (primarily Ni) to gasify the pyrolytic tars.[12,39−58] However, Ni and many of the other metals that have been shown to be active catalysts for tar gasification are subject to severe corrosion by supercritical water at the temperatures needed to secure high yields of hydrogen (see below). In the field of biomass conversion, downdraft gasifiers[59,60] are known for their ability to produce a tar-free gas. We assumed that this result derives from the flow of the hot, tar-laden gas through the bed of red-hot charcoal that exists in the bottom of most downdraft gasifiers. Consequently, we explored the use of charcoal and other carbons as catalysts for the gasification of tars in supercritical water and were rewarded by the observation of a clean water effluent from our reactor.[38] Although carbon is perceived to be an unlikely catalyst by many workers, there is an extensive literature on its use as both a catalyst support and a catalyst.[61,62] In our case, the carbon is particularly effective because it is stable in supercritical water at the temperatures employed in this work, particularly in the presence of hydrogen.[63,64] In this paper, we describe the use of a carbon catalyst to effect the steam reforming of wood sawdust and potato wastes to a hydrogen-rich gas. Extraordinary yields of gas (>2L/g) were realized under some conditions, with clean water as the major byproduct of the gasification chemistry.

Apparatus and Experimental Procedures

The three flow reactors (see Figures 1−3) used in this work were fabricated from Hastelloy C-276 tubing with 9.53 mm o.d. × 6.22 mm i.d. × 1.016 m length. The reactant flow was quickly heated by the entrance heater to temperatures as high as 800 °C. In some cases, the annular thermocouple well within reactors #1 and #2 was replaced by an electrical annulus heater (3.18 mm o.d. × 15.2 cm heated length). Downstream of the entrance heater, the reactor's temperature was maintained in an isothermal condition by an Applied Test Systems Series 3210 furnace. The chief purpose of the furnace was to prevent heat loss. In fact, in some experiments, the temperature set point of the furnace was below the lowest temperature measured along the reactor wall. Carbon catalyst (Barnebey and Sutcliffe Corp., type PE coconut-shell-activated carbon, ≥16 mesh, with a bulk density of 0.48 g/cm^3) was usually packed in about 60% of the heated zone of the reactor, as well as the downstream cold section of the reactor. Earlier work[38] showed that biomass charcoal (with a surface area below 50 m^2/g and a negligible pore volume) was more effective as a catalyst than activated carbon; consequently, we assumed that all of the catalytic gasification chemistry occurred on the activated carbon particles' outer surfaces (as was the case with the charcoal particles). Hence, we did not attempt to measure effectiveness factors for the activated carbon catalyst employed in this work. Note that we used activated carbon catalysts solely as a convenience because of their homogeneity, size, and availability. In some cases, alumina was substituted for carbon in the

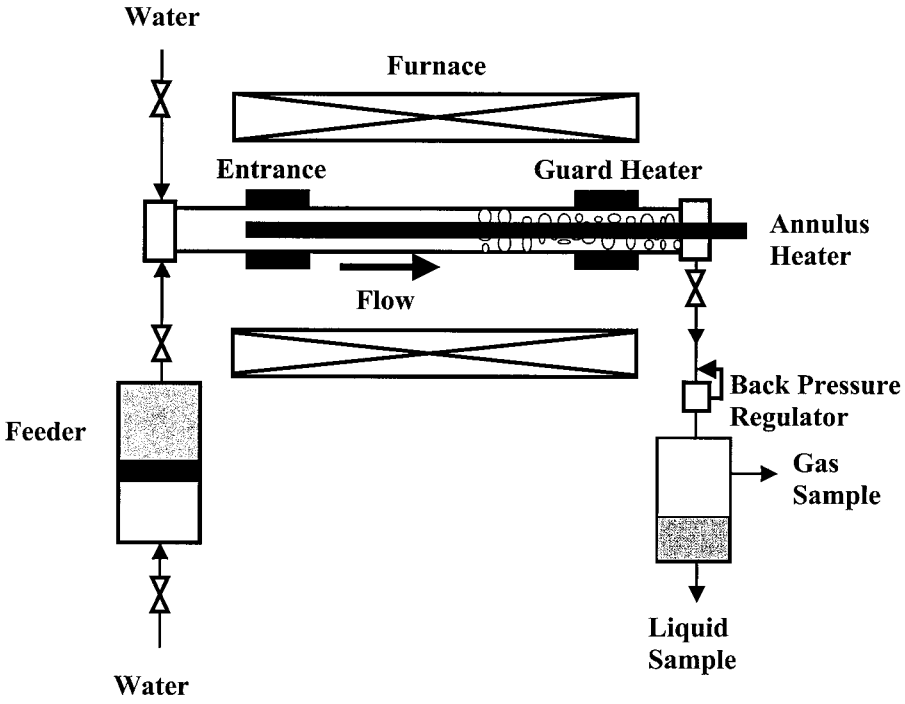

Figure 2. Schematic diagram of reactor #2. HPLC pumps and external cooling water jackets not shown.

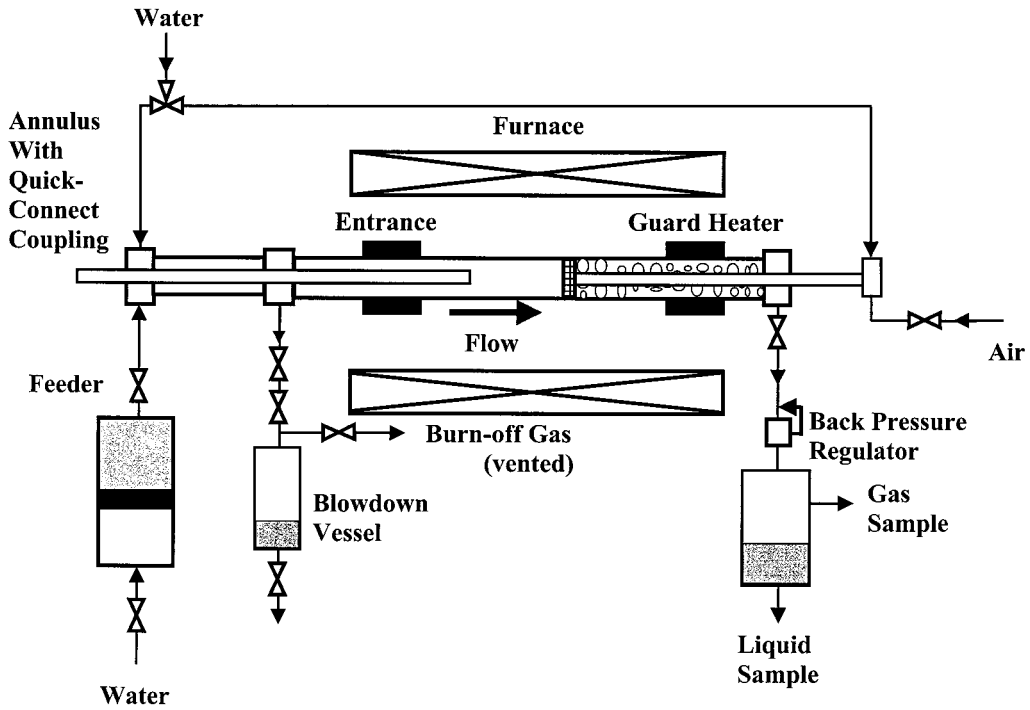

Figure 3. Schematic diagram of reactor #3, the reversible-flow, intermittent-purging reactor. HPLC pumps and external cooling water jackets not shown.

cold section of the reactor, while the heated zone was kept packed with carbon. This substitution had no measurable effect on the performance of the reactor. The reactor's temperature profile was monitored by 12 fixed, type K thermocouples held in good thermal contact with the reactor along its outer wall. Also, in reactors #1 and #3, the reactant temperature was measured by a fixed, internal annulus thermocouple. Pressure in the reactor was measured by an Omega PX302 pressure transducer. A Grove Mitey-Mite model 91 back-pressure regulator reduced the pressure of the cold, two-phase product effluent from 28 to 0.1 MPa. After leaving the back-pressure regulator, the reaction products passed through a gas−liquid separator. The liquid product was collected over a measured time period to calculate the liquid outlet flow rate. The gas flow rate was measured using a Sinagawa Corp. wet test meter.

Reactor #3 permitted intermittent removal of the deposits that caused plugging in reactors #1 and #2. After the onset of plugging (pressure drop of 0.7 MPa across the reactor), delivery of the reactant was halted. Water was then pumped through the reactor to flush residual reactant into the heated portion of the reactor and gasify it. The flow of water was terminated and the reactor depressurized by carefully releasing its contents into the blowdown vessel. Next, the reactor annulus was

Table 1. Elemental Analyses of Feedstocks[a]

element	cornstarch	poplar wood sawdust	potato starch	potato waste
C	42.7	49.4	42.5	44.1
H	6.2	6.0	6.4	5.7
O	50.9	45.1	50.8	37.9
N	0.1	0.1	0.0	2.8
S	0.1	0.0	0.0	0.3
ash	0.1	0.2	0.3	9.3
moisture content[b]	12.8	8.5	18.8	80[c]

[a] Elemental analyses are given as wt % (dry basis); the elemental analysis was conducted by Huffman Laboratories, Inc. [b] Moisture content (wet basis) was measured by placing the samples in an oven at 105 °C. [c] This is an approximate value.

removed by opening a quick-connect coupling, and the reactor was sealed again with a plug (also joined by a quick-connect coupling). Air at atmospheric pressure was delivered via the rear annulus (in reverse flow) past the carbon catalyst bed to the middle of the reactor. The carbon present in the deposit was burned by the flowing air, and the carbon dioxide content of the vented gas was monitored by an IR analyzer. The flow of air was stopped when the carbon dioxide content of the vented gas dropped to less than 0.2%. Next, the plug sealing the front of the reactor was removed. A soft metal brush was quickly inserted into the reactor and used to loosen ash and residual carbon that adhered to the reactor walls. After sealing the reactor again, air flow was resumed for a few minutes to blow the ash into the blowdown vessel. Finally, the front annulus was replaced within the reactor and the system pressurized with water. When a stable temperature profile was achieved, delivery of the reactant was resumed as described earlier. Typically, this cleanup procedure was accomplished in less than 30 min.

For the conditions employed in this work, flow within the reactor was laminar ($Re \approx 200$). Estimated residence times in the heatup zone, void (cracking) zone, and packed-bed zone of the reactor were about 20, 40, and 20 s, respectively, for a typical experiment with a flow of about 2 g/min of feed material.

Six different types of feedstocks were used in this work: glycerol, cornstarch and potato-starch gels, poplar wood sawdust and sugarcane bagasse suspended in a cornstarch gel, and potato wastes obtained from Lamb-Weston Corporation. A gel was made from dry starch powder by combining the starch with an amount of water slightly in excess of the desired amount (to make up for evaporation losses). The mixture was continually stirred and heated until it thickened and boiled. It was then mixed with ground sawdust and allowed to cool. The bagasse and poplar sawdust was ground with a Wiley mill (Thomas Scientific) to 40 mesh before it was mixed into the gel. The potato-waste feed was treated in a similar fashion. The raw potato waste was blended until it had a smooth consistency. Water was added, if necessary, to achieve the desired solids loading; then, the mixture was continually stirred and heated. It was allowed to boil for several minutes. Table 1 gives the results of elemental analyses of the feedstocks.

The feeder consisted of a cylinder, a movable piston, and two end-caps (High Pressure Equipment). The piston was placed in the center of the cylinder, the top of the cylinder was then filled with water, and the top end-cap was installed. Subsequently, the cylinder was inverted, the top filled with feedstock, and the second end-cap installed. Both the feeder and the reactor were pressurized separately to 28 MPa at the beginning of a run. During the time that the system was being brought up to temperature, water was delivered to the reactor by a Waters 510 HPLC pump. When the main body of the reactor reached the desired temperature (usually about 650 °C), the valve connecting the feeder to the reactor was opened. Thereafter, water flow to the reactor was terminated, and water flow to the feeder was initiated, displacing the gel feedstock into the reactor. Because the thermophysical properties of the gels are considerably different than those of pure water, and possibly also because of exothermic pyrolysis reactions associated with the decomposition of the gels, the temperature of the gel feed rose very rapidly during its entrance into the reactor. To avoid excessively high temperatures after the feed was switched from water to gel, usually it was necessary to reduce the heat input to the gel feed from the annulus heater and the entrance heater.

Gas samples were taken by gastight syringes from the gas sample outlet of the gas−liquid separator. These samples were sometimes injected into gastight vacutainers for short-term storage. Analysis of the gas was conducted using a Hewlett-Packard model 5890 gas chromatograph equipped with flame-ionization and thermal-conductivity detectors. A 80/100-mesh carbosphere molecular sieve packed column was used, operating at 35 °C for 4.0 min, followed by a 25 °C/min ramp to 350 °C, and a 1.4 min hold at 350 °C. The carrier gas was a mixture of 8% hydrogen in helium. A standard gas mixture was used for day-to-day calibration, and a method verification standard was used at the beginning and end of a sample set to verify the accuracy of the standard calibration. We remark that traces (<1 mol %) of ethane and higher hydrocarbons were detected in many gas samples but were not quantified. The COD of the liquid effluent was measured by a Hach model 45600 COD reactor.

Proton-induced X-ray emission (PIXE) analyses were performed by Elemental Analysis Corp. PIXE is a nondestructive analytical method that simultaneously quantifies 72 elements ranging from sodium through uranium. Under bombardment by protons, individual elements emit characteristic X-rays that are used to measure the concentrations present in a given sample. Depending on the sample composition, PIXE yields sensitivities in the mid parts per billion to the low parts per million range for most applications.

Microbeam Technologies, Inc. (MTI) analyzed a corroded Hastelloy reactor by backscattered electron imaging, energy-dispersive X-ray spectrometry (SEM), and scanning electron microscopy point count (SEMPC). The SEMPC method quantitatively determines the relative amount of elements present in ashes and deposits. It involves microprobe analysis (of chemical compositions) of a large number of random points taken from a polished cross section of a sample.

In what follows, we report gas yields as liters of gas at NTP (25 °C and 0.1 MPa) per gram of organic matter in the feedstock (L/g) and grams of gas per gram of organic matter in the feed (g/g), based on calculated gas concentrations and real-time gas flow measurements. The reported carbon efficiency is the mass of carbon in the gas divided by the mass of carbon in the feed. Because the biomass gels and potato wastes were not perfectly homogeneous, and because of variations in the gas flow rate due to unsteady release of gas by the back-

Table 2. Effects of Increasing Temperature and Flow Rate on Cornstarch Gasification

experiment date	2/20/97[a]			4/5/99[b]		
flow rate (g/min)	1.0	2.0	4.0	2.0	2.0	2.0
reactor peak temp (°C)	690	715	805	≥745	≥745	≥745
catalyst bed temp (°C)	650	650	650	715	715	715
time on stream (h)	2.18	4.57	5.70	0.45	0.73	1.00
product (mole fraction)						
H_2	0.37	0.37	0.47	0.55	0.57	0.55
CO	0.02	0.01	0.02	0.03	0.03	0.03
CO_2	0.38	0.42	0.37	0.35	0.34	0.35
CH_4	0.22	0.19	0.15	0.07	0.06	0.06
gas yield						
(L gas/g organics)	1.28	1.38	1.70	2.05	2.05	2.05
(g gas/g organics)	1.13	1.27	1.40	1.55	1.50	1.54
C efficiency	0.91	0.98	1.06	1.06	1.01	1.04
global mass balance	1.01	1.01	1.00	1.06	1.06	1.06
TOC in water[c]	0.5	0.3	0.4	NA[d]	NA	NA

[a] Feedstock is 10.4 wt % cornstarch; reactor #1 with annulus heater; 28 MPa. [b] Feedstock is 13.7 wt % cornstarch; reactor #1 with annulus heater that was not energized; 28 MPa. [c] Values represent percent by weight of carbon in feedstock. Total organic carbon (TOC) analyses of liquid effluent were measured by the Water Resources Research Center, University of Hawaii. [d] NA = not available.

pressure relief valve, the carbon efficiency occasionally exceeded 1.0 by a small amount. The reported global mass balance is based on the flow of water and gas leaving the reactor and the flow of feed entering the reactor.

A factorial experimental design was used for quantification of the effects of two important process parameters on the gas yield (reactor #3): the catalyst bed temperature and the weight hourly space velocity (WHSV). We report WHSV as the rate of delivery of organics to the reactor (g/min) divided by the mass of the carbon catalyst in the heated zone of the reactor. Each of these process parameters was evaluated at a lower and upper value (designated as levels 0 and 1, respectively). The gas yield was then determined for four different experimental conditions, each representing one of the four possible parameter combinations [for example, (1, 0) represents the gas yield obtained using the upper catalyst bed temperature and the lower WHSV]. The effect (difference in gas yield) obtained by varying each parameter from its lower to its upper value was then determined. In the case of catalyst bed temperature, effect no. 1 = (1, 0) − (0, 0) and effect no. 2 = (1, 1) − (0, 1). The mean effect of the variation in catalyst bed temperature on the gas yield was then calculated as the average of these two effects.

Results and Discussion

Starch Gels. Table 2 displays gasification results obtained with increasing flow rates of 10.4 wt % cornstarch gel feed. To deliver sufficient heat to the reactant at the higher flow rates, the reactor peak temperature was increased from 690 to 805 °C. This increase in temperature, combined with the decrease in residence times and increase in weight hourly space velocity (WHSV), influenced both the gas yield and the gas composition. The higher temperatures drove the methane steam-reforming reaction to increase hydrogen yields at the expense of methane. Because the methane steam-reforming reaction created 5 mol of product gas from 3 mol of reactant, the carbon dioxide mole fraction of the gas product also decreased. Note that the gas yield reached 1.7 L/g at the highest peak temperature. On a mass basis, these yields reached 1.4 g gas/g organics, indicating the consumption of water by the gasification reactions. This consumption of water was plainly evident to students and staff involved in the experiment and is manifest in the good mass balances. The water that left the reactor was clean with a pH of 7 and TOC values that represented 0.3−0.5 wt % of the carbon content of the feed. To an observer, the most convincing evidence of the effectively complete gasification of the starch feed was the clear, almost odor-free water that left the reactor. Except for a few runs, which involved a malfunctioning pressure relief valve (see below), the water effluent of the reactor was clear for all of the experiments described in this paper.

Table 3. Effects of High Temperatures and Reactor "Seasoning" on Gasification[a]

experiment date	7/3/97	7/10/97
feedstocks	10.72 wt % sawdust/ 4.01 wt % cornstarch	11.17 wt % sawdust/ 4.19 wt % cornstarch
reactor peak temp (°C)	790	790
catalyst bed temp (°C)	685	690
time on stream (h)	1.62	1.52
product (mole fraction)		
H_2	0.43	0.57
CO	0.03	0.04
CO_2	0.38	0.33
CH_4	0.17	0.06
gas yield		
(L gas/g organics)	1.61	2.18
(g gas/g organics)	1.39	1.58
C efficiency	0.96	0.97
global mass balance	1.01	1.00

[a] Flow rate, 2.0 g/min; reactor #1 with annulus heater; 28 MPa.

Table 2 also presents a more extreme "high-temperature" gasification result (experiment dated 4/5/99). The gas yield (2 L/g) and gas composition (55% hydrogen, 35% carbon dioxide, and 6% methane) realized in this experiment are extraordinary. Unfortunately, our equipment did not permit an accurate measurement of the peak temperature during this run. After the experiment was completed and the reactor was disassembled, we detected a slight bulge in the reactor tube under the entrance heater. This bulge suggested that the entrance temperature was considerably higher than the registered peak temperature.

Biomass/Starch Gels. Viscosities of the sawdust-laden starch gel and potato-waste feedstocks were measured by Brookfield Engineering using their CPS rheometer. To acquire meaningful data for a variety of applications, profiles of shear rate vs viscosity for each mixture were measured to a maximum shear rate of 120/s. The maximum measured viscosity of the sawdust gel was about 9 000 cP, whereas the maximum value for the potato wastes was 16 000 cP. In both cases, the viscosity decreased with increasing shear rate.

High-temperature gasification results for sawdust mixed in a cornstarch gel from two consecutive runs (no intervening experiments) on different days are displayed in Table 3. In both cases, the effluent water was clean with a pH of 7−7.5, but the reactor plugged after 2−3 h on stream. Although the measured temperatures were similar on July 3 and July 10, the gas yield increased from 1.61 to 2.18 L/g, and the hydrogen content of the gas increased from 43 to 57%. Because fresh carbon catalyst was employed with each experiment, we attribute the increase in gas yield to a seasoning effect (corrosion) of the high temperature in the entrance region on the reactor's wall. It is also possible that the peak temperature of the reactor on July 10 was significantly higher than the temperature recorded by the single thermocouple.

Table 4. Gasification with Low Peak Temperature[a]

experiment date	12/17/97	4/21/98
feedstocks	9.47 wt % sawdust/ 3.55 wt % cornstarch	10.64 wt % sawdust/ 3.88 wt % cornstarch
reactor peak temp (°C)	750	739
catalyst bed temp (°C)	700	710
time on stream (h)	1.37	1.95
product (mole fraction)		
H_2	0.27	0.26
CO	0.02	0.02
CO_2	0.46	0.46
CH_4	0.24	0.23
gas yield		
(L gas/g organics)	1.36	1.15
(g gas/g organics)	1.40	1.18
C efficiency	1.01	0.84
global mass balance	0.95	1.00

[a] Flow rate, 2.0 g/min; reactor #2; 28 MPa.

Table 4 displays lower-temperature gasification results from reactor #2. Because of the lower temperatures, the hydrogen content of the gas was only 26−30%, and the gas yield was lower (1.15−1.36 L/g). However, in both cases, the water was clean and had a pH of 7. Corroborating this observation, the measured COD value of the water effluent from experiment 4/21/98 was 56 mg/L.

Results from a study of the effects of total pressure on the gasification of sugarcane bagasse in a cornstarch gel showed that an increase in pressure from 28 to 34.5 MPa had no significant effect on the gas composition or yields.

The data for cornstarch and poplar wood were analyzed with respect to chemical equilibrium. In this analysis, both STANJAN and HYSIM were used to calculate the equilibrium concentrations of H_2, CO_2, CO, water, methane, and ethane. STANJAN calculates the equilibrium mole fractions on the basis of thermodynamic principals assuming the ideal gas law applies. HYSIM performs the same calculation; however, it uses Peng−Robinson equations of state to correct for nonideal conditions. A comparison of the two results shows that STANJAN tends to overpredict the equilibrium concentration of hydrogen and underpredict the concentration of methane under these supercritical conditions.

Figure 4 shows a plot of the results of this analysis. The *x* axis of Figure 4 displays the mole fractions calculated by HYSIM on a dry basis using Peng−Robinson equations of state. The *y* axis displays the measurements made during this study for mixtures of cornstarch and cornstarch with poplar wood. Note that the equilibrium mole fraction for ethane under these operating conditions was zero. The data in Figure 4 show that the hydrogen mole fractions fall on both sides of the equilibrium concentrations. Furthermore, the tests for which hydrogen is below equilibrium are the same tests for which methane is above equilibrium. This indicates that the reactions are capable of proceeding in such a way as to approach equilibrium of hydrogen and methane from either side. Clearly, methane is being formed at the expense of hydrogen.

Figure 5 shows a plot of the hydrogen yield, in liters per gram of solid feed, as a function of the peak reactor temperature for the data shown in Figure 4. This figure shows that higher peak reactor temperatures, and therefore faster heating rates during the approach to the critical temperature, favor hydrogen formation. It appears that slower heating rates favor the formation of refractory compounds (e.g., acetic acid), which results in more methane production. The large differences in hydrogen yields evidenced by points 3−6 are a result of seasoning effects due to high peak temperatures (see Tables 2 and 3).

Potato Wastes. Table 5 compares results from the gasification of commercial potato waste, potato starch, and cornstarch using reactor #1 with an annulus heater and with a short thermocouple well annulus (not an annulus heater). As expected, slightly higher gas yields were obtained with the annulus heater, but the gas compositions were nearly identical. We remark that the cornstarch experiment with a solids loading of 8.9% proceeded for more than 3 h without plugging, whereas the cornstarch experiment with a solids loading of 13.1% plugged after 2 h.

The influence of two important process parameters, the catalyst-bed temperature and the WHSV, was examined using a 2-parameter factorial experimental design. Potato starch was chosen as the feedstock. Because of its homogeneity, high purity, and low ash content, it serves as a model compound for the potato-waste feedstock. The results are summarized in Table

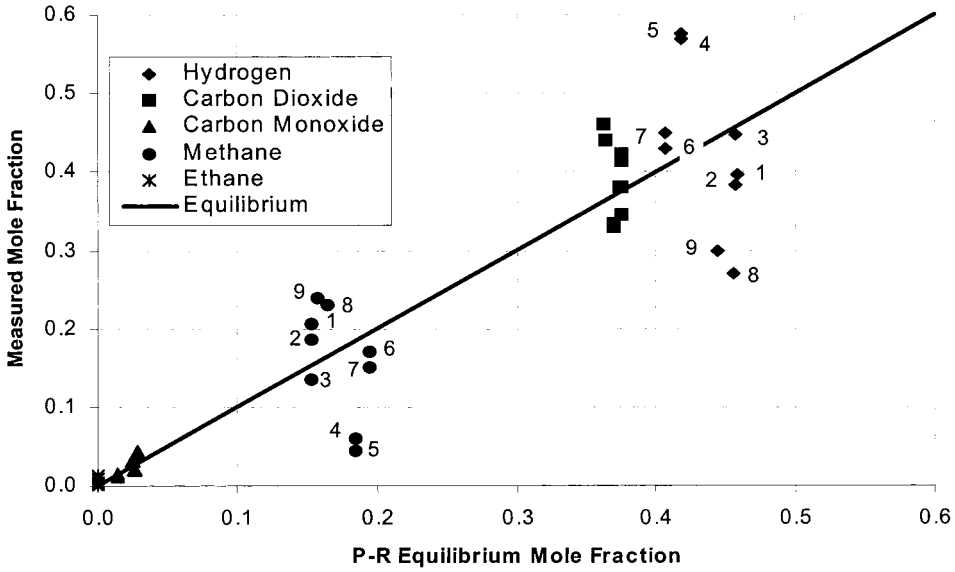

Figure 4. Comparison of test measurements to equilibrium at catalyst temperatures. Test dates for points: 1, 2/20/97; 2, 2/20/97; 3, 2/20/97; 4, 7/3/97; 5, 7/10/97; 6, 7/10/97; 7, 7/21/97; 8, 12/18/97; 9, 2/12/98.

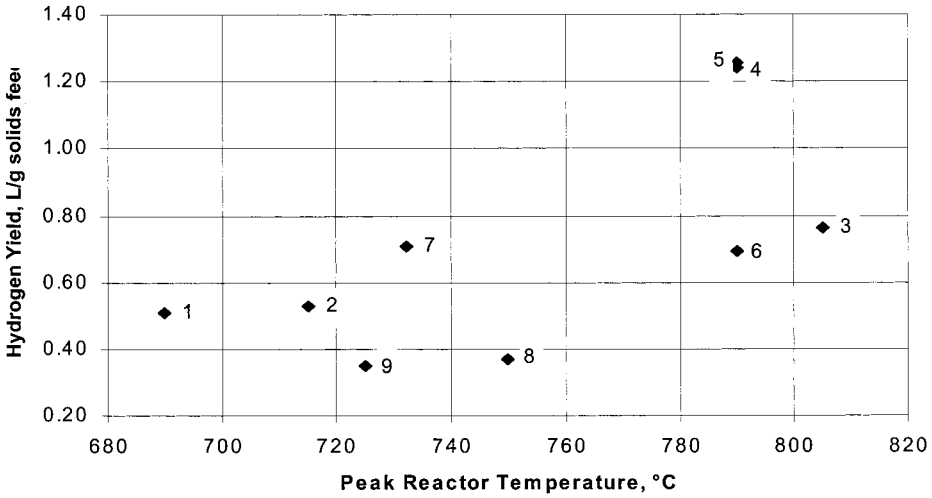

Figure 5. Hydrogen yield versus peak reactor temperature. Test dates for points: 1, 2/20/97; 2, 2/20/97; 3, 2/20/97; 4, 7/3/97; 5, 7/10/97; 6, 7/10/97; 7, 7/21/97; 8, 12/18/97; 9, 2/12/98.

Table 5. Comparison of Cornstarch, Potato-Starch, and Potato-Waste Gasification[a]

experiment date	3/8/99[b]	4/13/99[c]	3/30/99[b]	4/15/99[c]	3/16/99[b]	4/20/99[c]
solids loading (wt %)	8.9	13.1	11.9	12.8	13.4	13.7
feedstock	cornstarch		potato starch		potato waste	
reactor peak temp (°C)	711	713	714	700	719	705
catalyst bed temp (°C)	708	717	715	717	724	718
time on stream (h)	1.35	1.35	0.85	0.98	0.58	1.15
product (mole fraction)						
H_2	0.33	0.29	0.31	0.31	0.32	0.33
CO	0.01	0.03	0.01	0.01	0.01	0.01
CO_2	0.46	0.47	0.47	0.49	0.44	0.45
CH_4	0.19	0.18	0.21	0.17	0.21	0.19
gas yield						
(L gas/g organics)	1.10	1.04	1.12	0.91	1.07	1.00
(g gas/g organics)	1.09	1.06	1.14	0.94	1.04	0.97
C efficiency	0.83	0.81	0.89	0.70	0.79	0.72
global mass balance	1.01	1.02	1.01	0.97	0.97	0.98

[a] Flow rate, 2.0 g/min; reactor #1; 28MPa. [b] Annulus heater. [c] 1/8-in. o.d. Inconel tube as the annulus.

Table 6. Effect of Process Parameters on Gasification[a]

experiment date	9/21/99	9/23/99	9/21/99	9/23/99
feedstocks	13.3 wt % potato starch	14.4 wt % potato starch	13.3 wt % potato starch	14.4 wt % potato starch
reactor peak temp (°C)	750	760	750	750
catalyst bed temp (°C)	690	690	750	750
WHSV[b] [(g/h)/g]	4.8	11.3	4.8	11.3
time on stream (h)	1.08	1.18	1.15	1.28
gas yield				
(L gas/g organics)	0.82	0.95	1.13	1.00
(g gas/g organics)	0.80	0.94	1.13	1.00
C efficiency	0.63	0.74	0.89	0.79
global mass balance	0.99	1.02	1.07	1.02
process parameter	catalyst bed temp		WHSV[b]	
variation	690−750 °C		4.8−11.3 (g/h)/g	
mean effect of the variation on gas yield[c] (g gas/g organics)	0.20		0	

[a] Flow rate, 2.0 g/min; reactor #3; 28 MPa. [b] WHSV is weight hourly space velocity. [c] The mean effect of a variation on the gas yield (g gas/g organics) is the average of the differences in the gas yield resulting from that variation for all the conditions evaluated (see Apparatus and Experimental Procedures for sample calculation). Mean effects within the experimental error of 0.08 g gas/g organics (standard deviation of the gas yield from three identical experiments) are listed as 0.

6. In all cases, gasification was complete, and the mole fractions of hydrogen, carbon dioxide and methane were approximately 0.33, 0.45, and 0.18, respectively. Increasing the catalyst-bed temperature from 690 to 750 °C had a significant, positive effect on the gas yield. This result again shows the importance of the reaction temperature on the gasification. The substitution of a portion of the carbon catalyst bed with alumina increased the WHSV, while keeping the bed volume constant. Doubling the WHSV had little effect on the gas yield or composition. This result is encouraging as it shows the potential for gasification at a much higher throughput.

Figure 6 displays the results from the gasification of commercial potato waste during an 8-h run. The feed had solids loadings of 10−18 wt %. The run required eight individual feeding cycles, between which carbon and ash deposits were removed from the reactor. The average gas composition did not change greatly from one cycle to the next, but the total gas yield and gas energy

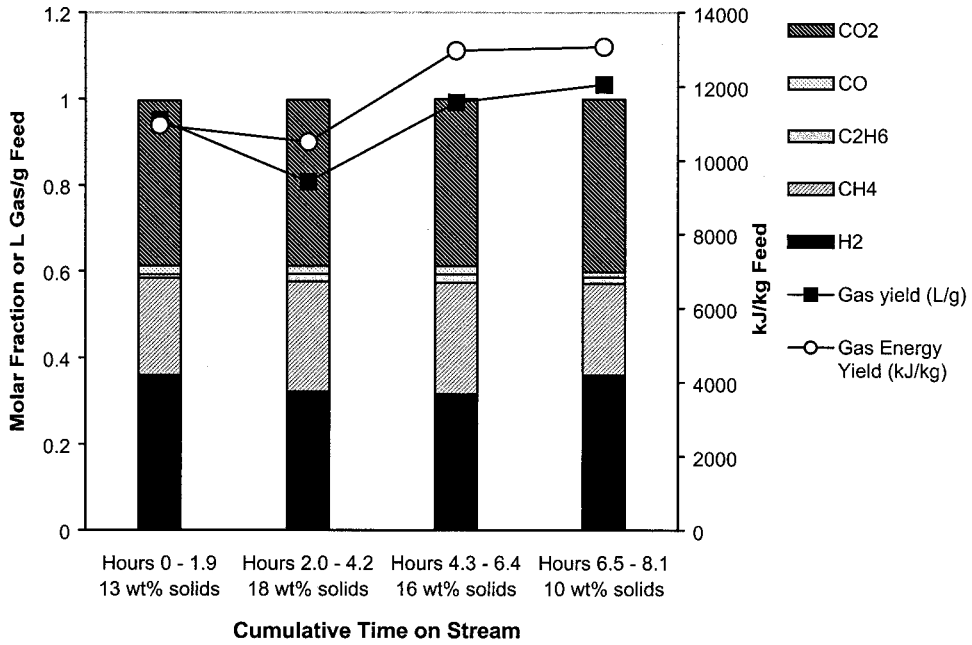

Figure 6. Gas composition, gas yield, and gas energy yield for potato-waste gasification using reactor #3 at 2.0 g/min and 28 MPa over an 8-h period.

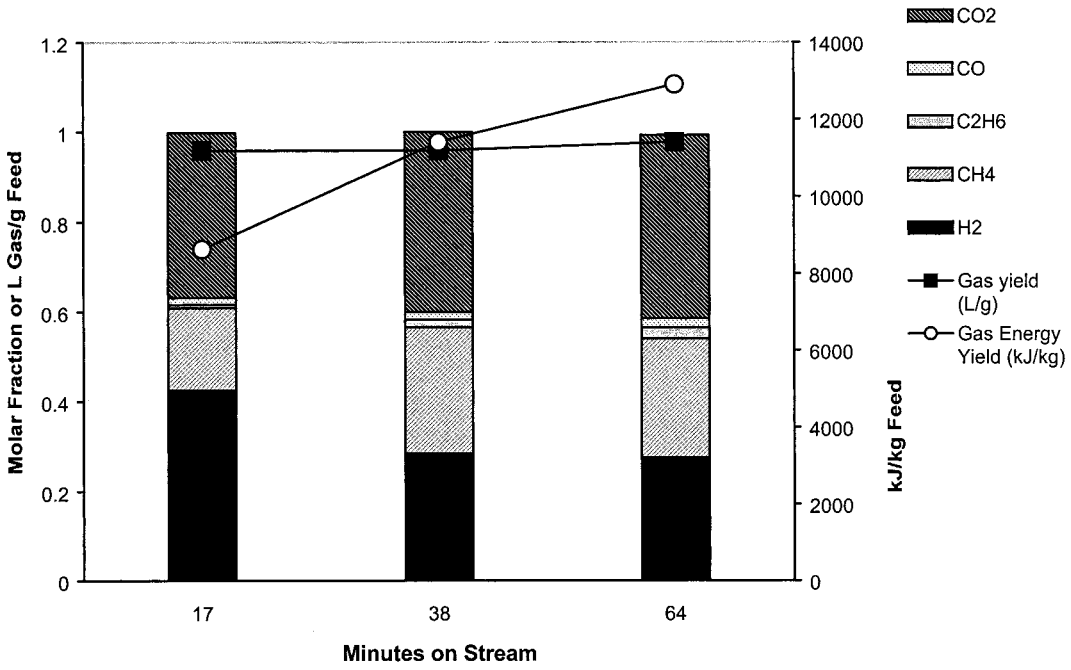

Figure 7. Changes in the gas composition, gas yield, and gas energy yield for potato-waste gasification using reactor #3 at 2.0 g/min and 28 MPa over the course of a cycle. Data is an average of seven individual feeding cycles.

yield (kilojoules of gas energy per kilogram of organics in feed) increased with time on stream. Figure 7 displays the average gas composition measured at different times during each of seven cycles. Data from the eighth cycle was not included because it was of short duration. Note that the hydrogen content of the gas decreased with time, whereas the methane, carbon dioxide, and ethane contents all increased. Despite this variation in the gas composition, the gas yield during the cycle remained nearly constant. We assume that the changes in gas composition are due to carbon and ash buildup on the wall of the reactor, which reduced access of the reactant to the catalytic metal content of the reactor's wall. Figure 8 offers insight into the effects of plugging on heat transfer to the reactant during a cycle. As shown in Figure 8, temperatures along the length of the reactor fall by about 10 °C over the course of a cycle. This phenomenon can be explained by the reduction in heat transfer across the wall of the reactor associated with char and ash deposition in the heatup zone of the reactor. Lower temperatures within the reactor reduce hydrogen production.

Significant changes were observed in the activated carbon catalyst during the 8-h experiment. The measured BET surface area of the carbon decreased from 980 to 270 m^2/g after 8 h time on stream, and its packing density increased from 0.474 to 0.523 g/mL. Table 7 compares the elemental analyses of the spent activated carbon catalyst with the carbon as received from the manufacturer. The carbon and the oxygen content of the

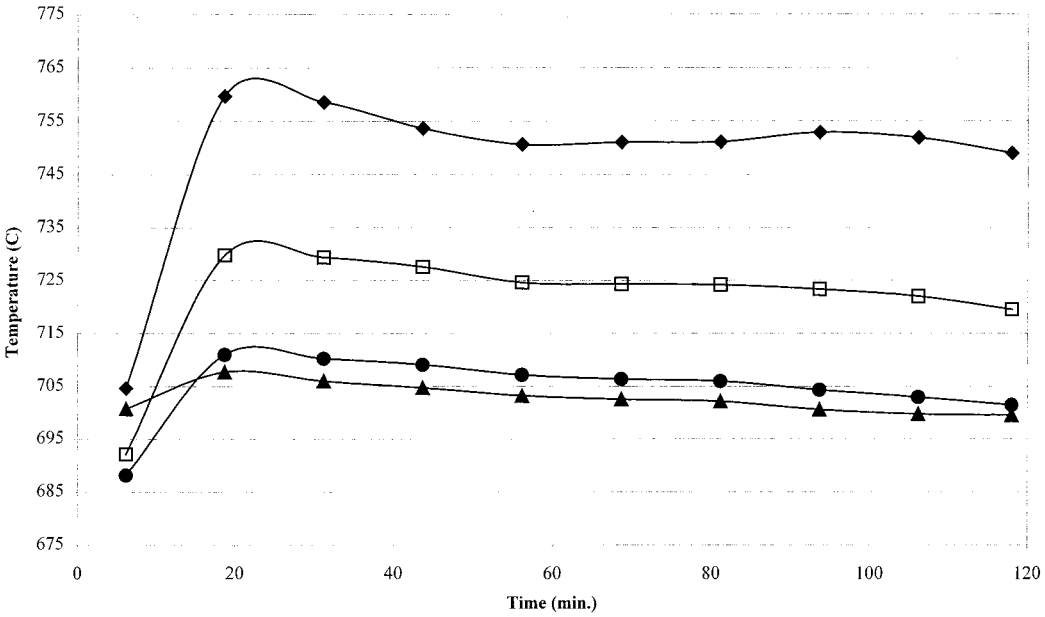

Figure 8. Temperature variation over a gasification cycle. Thermocouples are located ◆, 3 in. past the entrance heater; □, 5 in. past the entrance heater; ●, 7 in. past the entrance heater; and ▲, 9 in. past the entrance heater on the exterior of the reactor. Experiment date is 10/08/99 (cycle #1). Timing begins at the start of the cycle.

Table 7. Elemental Analysis of Coconut-Activated Carbon[a]

	as received	8 h on stream[b]
C	93.74	92.37
H	0.88	1.02
O	3.44	2.23
N	0.13	0.4
S	0.02	0.08
ash	1.79	5.21

[a] Elemental analyses are given as wt % (dry basis); the elemental analysis was conducted by Huffman Laboratories, Inc. [b] Used as a catalyst during experiments 991001, 991005, 991007, and 991008 with potato-waste feedstock.

catalyst decreased by about 1.2%, whereas the ash content increased by 3.4%. Proton-induced X-ray emission (PIXE) studies were also utilized to analyze both the as received and the spent (8 h on stream) activated carbon catalyst. As displayed in Table 8, the ash content of the spent carbon includes unexpectedly high amounts of Ni, Cr, Mo, and W. These metals are the prime constituents of the Hastelloy reactor tube. Their presence in the carbon catalyst signals the importance of corrosion of the reactor wall during the 8-h experiment (see below). Iron is present in the potato-waste feedstock (as well as Hastelloy); consequently, its appearance in the carbon catalyst is not surprising.

Wall Effects and Corrosion. Hastelloy C-276 is composed of Ni, as well as Mo, Cr, Co, and other metals (see Table 8), which can exert a catalytic influence on the gasification chemistry. One approach to studying the catalytic role of the reactor's wall is to run a sequence of feedstocks, such as glycerol in water, followed by glucose in water, followed by glycerol in water. Glycerol is easily gasified, and the gas composition is affected by the condition of the reactor's wall. In this way, glycerol can be used to probe the influence of the reactor's wall on the gasification chemistry. This approach is illustrated in Table 9, which shows that the gasification of 22.5 wt % glucose for 3.68 h did not alter the gas composition derived from glycerol. On the other hand, the gasifications of Avicel cellulose in a cornstarch gel (see Table 10) and Kraft lignin in a cornstarch gel (see Table 11) reduced the role of the steam-reforming reaction, as evidenced by the decrease in hydrogen and the increase in methane in the gas derived from glycerol. These changes in gas composition can be attributed to carbon buildup on the reactor wall, which reduced the catalytic effects of the metallic wall on the gasification chemistry. Carbon buildup was especially evident with the lignin feed, which plugged after only 10 min and offered a very low gas yield.

As mentioned earlier, plugging due to carbon and ash buildup usually occurred with the sawdust paste after 2−3 h on stream. Often, we removed the plug by pumping a 1.2 M solution of hydrogen peroxide into the reactor for a short time. Table 12 gives results from the high-temperature gasification of sawdust starch gel before and after the reactor was cleaned using hydrogen peroxide. Both the very high gas yield and the high hydrogen content were retained after cleaning. In fact, the cleaning with hydrogen peroxide seemed to reduce the presence of hydrocarbons in the gas. These results are also consistent with the hypothesis that carbon buildup (which inhibits access of the reactant to the catalytic wall of the reactor) is the primary cause for changes in gas composition and yield during a run.

Evidence suggests that the ash content of the feed affects the length of time required for the reactor to plug. At similar solids loadings, the potato wastes (with 9% ash) plugged in one-half the time required by either the corn- or the potato-starch gels (with 1% ash). We recovered the solid material (derived from the potato-waste feed) that adhered to the wall of reactor #3 after rinsing and burnoff by air at atmospheric pressure. This material was analyzed by the Huffman Laboratory and determined to be 91% ash. The composition of this "reactor residue" is compared with the composition of ash taken directly from the potato waste (without gasification) in Table 8. Note that there is no Ni in the potato-waste ash. Both the ICP and the PIXE analyses indicated a high concentration of Ni in the ash taken from the reactor. In addition, the PIXE analysis revealed that the ash taken from the reactor contained all of the elements present in the Hastelloy alloy. As

Table 8. Analysis of Ash and Activated Carbon Catalyst[a]

	manufacturer's specifications	PIXE analysis[b]			ICP analysis[c]	
	Hastelloy	AC, as received[d]	AC, 8 h on stream[e]	reactor residue[f]	reactor residue ash[c]	potato-waste ash
Na	0	8.4	0.0	0.0	1.3	2.5
Mg	0	3.5	4.7	10.2	13.9	8.0
Al	0	0.0	1.7	1.1	4.5	5.9
Si	0.1[g]	6.8	4.4	2.1	19.7	29.8
P	0	2.3	4.8	10.2	17.9	14.2
S	0	2.7	1.6	3.2	0.2	3.5
Cl	0	0.0	0.4	0.0	NA[i]	NA
K	0	70.7	10.3	1.0	4.8	23.0
Ca	0	4.4	4.8	8.6	11.8	8.9
Cr	16	0.0	11.6	11.7	NA	NA
Mn	1[g]	0.0	0.5	0.6	0.3	0.1
Fe	5	0.1	8.1	5.4	6.9	3.5
Ni	57[h]	1.1	47.0	42.8	18.3	0.0
Mo	16	0.1	10.6	2.1	NA	NA
Co	3[g]	0.0	0.0	0.5	NA	NA
Cu	0	0.0	0.2	0.0	NA	NA
W	4	0.2	3.1	0.3	NA	NA
Ti	0	0.0	0.1	0.1	0.4	0.5

[a] All values are expressed as wt %. [b] The PIXE analysis was conducted by Elemental Analysis Corp. Values have been normalized to 100 wt % on a C-free basis. As analyzed by PIXE, reactor residue is 97.1% C, activated carbon after 8 h on stream is 96.2% C, and activated carbon as received is 99.0% C. [c] The ICP analysis was conducted by Huffman Laboratories, Inc. Values have been normalized to 100%. All elements are reported as oxides on ashed samples. Reactor residue is 91.1% ash, and the potato waste is 2.03% ash. Other metals or anions that were not detected by this analysis may be present in samples. [d] Activated carbon as received from manufacturer. [e] Activated carbon after 8 h of use. [f] Residue collected from reactor interior wall after plugging. [g] Maximum. [h] As balance. [i] NA = the technique does not detect this element.

Table 9. Absence of Reactor Wall Effects in the Gasification of Glycerol and Glucose Feedstocks[a]

feedstocks	18.71 wt % glycerol[b]	22.52 wt % glucose[c]	18.71 wt % glycerol
reactor peak temp (°C)	746	745	744
catalyst bed temp (°C)	710	707	707
time on stream (h)	1.79	3.68	5.01
product (mole fraction)			
H_2	0.52	0.46	0.52
CO	0.04	0.04	0.04
CO_2	0.32	0.36	0.31
CH_4	0.12	0.13	0.12
gas yield			
(L gas/g organics)	1.58	1.42	1.63
(g gas/g organics)	1.18	1.16	1.18
C efficiency	0.95	0.92	0.96
global mass balance	0.94	1.03	0.98

[a] Flow rate, 2.0 g/min; reactor #2; 28 MPa; experiment date, 6/17/98. [b] Water effluent COD was 54 mg/L. [c] Water effluent COD was 39 mg/L.

Table 10. Reactor Wall Effect in the Gasification of Glycerol and Avicel/Cornstarch Feedstocks[a]

feedstocks	18.71 wt % glycerol	11.43 wt % Avicel/ 4.57 wt % cornstarch	18.71 wt % glycerol
reactor peak temp (°C)	748	756	756
catalyst bed temp (°C)	718	715	715
time on stream (h)	1.62	2.70	4.24
product (mole fraction)			
H_2	0.51	0.30	0.45
CO	0.04	0.02	0.03
CO_2	0.31	0.45	0.32
CH_4	0.13	0.21	0.18
gas yield			
(L gas/g organics)	1.47	1.09	1.38
(g gas/g organics)	1.08	1.09	1.06
C efficiency	0.89	0.83	0.92
global mass balance	1.04	1.02	1.00

[a] Flow rate, 2.0 g/min; reactor #2; 28 MPa; experiment date, 5/14/98.

expected, the PIXE analysis also confirmed that the reactor residue contained nearly all of the minerals present in the potato-waste ash. Taken together, these findings are a clear indication of the breakdown of the Hastelloy alloy during gasification.

Table 11. Reactor Wall Effect Shown in the Gasification of Glycerol and Kraft Lignin/Cornstarch Feedstocks[a]

feedstocks	18.71 wt % glycerol	10.76 wt % Kraft lignin/ 4.25 wt % cornstarch[b]	18.71 wt % glycerol
reactor peak temp (°C)	758	757	758
catalyst bed temp (°C)	710	710	710
time on stream (h)	1.17	1.77	3.02
product (mole fraction)			
H_2	0.49	0.48	0.39
CO	0.03	0.02	0.03
CO_2	0.35	0.47	0.36
CH_4	0.13	0.02	0.21
gas yield			
(L gas/g organics)	1.45	0.39	1.30
(g gas/g organics)	1.15	0.36	1.11
C efficiency	0.93	0.15	0.98
global mass balance	1.00	NA	0.98

[a] Flow rate, 2.0 g/min; reactor #2; 28 MPa; experiment date, 8/27/98. [b] When lignin/cornstarch feedstock was used, the reactor plugged in 10 min. The liquid sample was too small to collect; as a result, the mass balance is not available.

Analysis of the Hastelloy reactor tubing by SEM confirmed that severe corrosion occurs during gasification. Figures 9 and 10 present backscattered electron microscope images displaying cross-sectional areas of the corrosion products on the reactor's inner wall. Two distinct layers are visible: the outer (i.e., nearest to the reactant) porous layer, which is extremely dark, and the inner (i.e., farthest from the reactant) layer, which is lighter in color than the outer layer but still darker than the base metal. The light and dark areas in the photographs represent chemically distinct zones. The thin, intact inner layer was rich in the metals that compose Hastelloy (Ni, Cr, etc.), whereas the outer layer was rich in the metals present in the potato-waste ash (Mg, Ca, K, and Si). Energy-dispersive X-ray spectrometry (SEM) was used to quantify the metal at individual points. There was considerable variation in the elemen-

Table 12. Effect of H_2O_2 Cleaning on Sawdust Gasification[a]

reactor peak temp (°C)	790		805	
catalyst bed temp (°C)	690		690	
	before plug		after plug and H_2O_2	
time on stream (h)	0.78	1.52	2.92	3.13
product (mole fraction)				
H_2	0.56	0.57	0.59	0.56
CO	0.04	0.04	0.04	0.05
CO_2	0.34	0.33	0.33	0.34
CH_4	0.06	0.06	0.04	0.05
gas yield				
(L gas/g organics)	2.18	2.18	2.18	2.18
(g gas/g organics)	1.62	1.58	1.56	1.63
C efficiency	0.99	0.97	0.92	0.99
global mass balance	1.00	1.00	0.99	0.97

[a] Feedstock is 11.17 wt % sawdust/4.19 wt % cornstarch at 2.0 g/min; reactor #1 with annulus heater; 28 MPa; experiment date, 7/10/97.

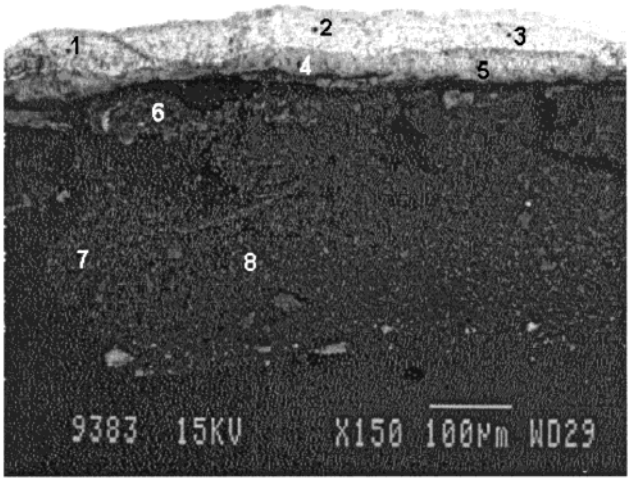

Figure 9. Backscattered electron image of corrosion product on inner diameter of used Hastelloy reactor, at 150× magnification, showing analysis points 1−8. The unaltered tube metal is the brightest layer at the top of the image.

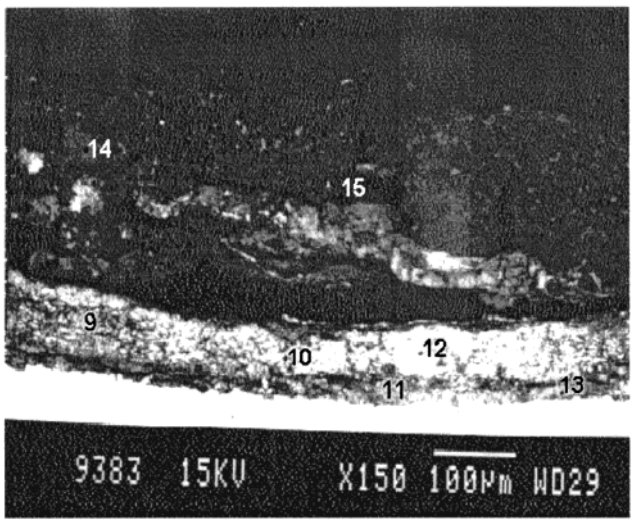

Figure 10. Backscattered electron image of corrosion product on inner diameter of used Hastelloy reactor, at 150× magnification, showing analysis points 9−15. The unaltered tube metal is the brightest layer at the bottom of the image.

tal composition of the different point areas that were analyzed (see Table 13). Nickel concentrations ranged from 0 to 55 wt %, Mo from 0 to 2.6 wt %, and Cr from 0 to 23 wt %. All of the metals contained in Hastelloy, except Fe, were depleted in the outer corrosion product layer. In fact, this layer appeared to be a deposit of ash and char annealed to the surface of the reactor, rather than Hastelloy. It is understandable that Fe was not depleted in this layer, as the potato-waste feedstock also contained Fe (see Table 8). Ni and Cr were enriched in the inner corrosion zone, and Mo was depleted in this zone. The base metal, on the other hand, was enriched in Mo and depleted of Ni when compared to the manufacturer's specifications. These observations were corroborated by the scanning electron microscopy point count (SEMPC) data listed in Table 14, which represent average values of 150 analysis points (similar to those listed in Table 13) for each layer.

PIXE analysis was performed on an adjacent piece of the same reactor. The results (Table 14) further substantiate the conclusion that metals were leached from the Hastelloy reactor's wall. The data revealed an increased concentration of Ni and a depletion of Mo and W in the inner corrosion layer. However, with the PIXE data, this phenomenon was not as pronounced as with SEMPC data. Also, trace amounts of the feedstock ash were detected by PIXE. Taken together, the SEM and PIXE analyses indicate that high-nickel alloys (e.g., Hastelloy, Inconel) are not suited for use in this application. The results also support the hypothesis that metals from the reactor wall may catalyze the observed gasification reactions.

Conclusion

A semisolid gel can be made from 4 wt % (or less) starch in water. Wood sawdust and other particulate biomass can be mixed into this gel and suspended therein for a period of days. This suspension is easily and reliably delivered to a supercritical flow reactor by a cement pump.

Above the critical pressure of water, the biomass-laden gel can be steam reformed over a carbon catalyst to a gas composed of hydrogen, carbon dioxide, methane, carbon monoxide, and traces of ethane. There are effectively no tarry byproducts. The liquid water effluent from the reactor has relatively low TOC and COD values, a pH between 3 and 8, and little or no color.

The gas composition and gas yield are strongly affected by the reaction temperature. High entrance temperatures favor the methane steam-reforming reaction and result in the production of a hydrogen-rich gas with yields exceeding 2 L/g. Other parameters, such as pressure, gas-phase residence time, and WHSV, exert a lesser influence on the reactor's performance.

The flow of feed into the reactor is eventually halted by a buildup of coke and ash in the heatup zone of the reactor. The coke is easily and quickly removed from the reactor by combustion in flowing air at 0.1 MPa. The ash is easily removed with a brush. Following this cleanup procedure, the reactor can be restarted.

Metals present in the Hastelloy reactor tube (i.e., Ni) appear to catalyze the gasification and reforming reactions. Some biomass feedstocks (e.g., Avicel and potato wastes) deactivate the reactor's wall.

Nickel alloy tubes (i.e., Hastelloy) are not suitable for use in this application. Hastelloy suffers severe corrosion under the conditions employed in this work. Metals leached from the Hastelloy are found in the activated carbon catalyst bed within the reactor.

Future work should be conducted in reactors with walls that do not suffer corrosion and do not catalyze

Table 13. Summary of Results from Energy Dispersive X-ray Spectroscopic Analysis of the Reactor's Interior Surface[a]

figure #	point #	description	Mg	Al	Si	S[b]	Cl	K	Ca	Cr	Fe	Ni	Mo	O
9	1	inner i.d. layer	0	0	0	0	0	0	0	10	3	52	2	33
	2	inner i.d. layer	0	0	0	0	0	0	0	23	5	18	3	51
	3	inner i.d. layer	0	0	0	0	0	0	0	9	3	46	1	40
	4	inner i.d. layer	0	1	0	0	0	0	0	9	3	37	2	48
	5	inner i.d. layer	0	0	0	0	0	0	2	11	3	22	0	62
	6	outer i.d. material	0	0	0	0	0	0	0	8	3	12	0	77
	7	outer i.d. material	9	0	0	0	0	3	21	0	1	0	0	67
	8	outer i.d. material	19	0	1	0	0	3	2	0	3	0	0	72
10	9	inner i.d. layer	0	0	1	0	0	0	0	10	3	13	0	72
	10	inner i.d. layer	0	0	0	0	0	0	0	3	1	55	1	39
	11	i.d. at tube interface	0	0	0	0	0	0	0	8	3	11	1	76
	12	inner i.d. layer	0	0	1	0	0	0	0	14	4	21	0	58
	13	i.d. at tube interface	0	0	0	0	0	0	0	10	3	12	0	74
	14	outer i.d. material	5	3	1	0	0	2	1	0	0	1	0	88
	15	outer i.d. material	0	0	0	0	7	0	0	0	0	0	0	93
none		base metal point	0	1	2	2	0	0	0	15	5	55	19	0
		base metal point	0	2	3	1	0	0	0	15	5	53	21	0
		base metal point	0	2	2	0	0	0	0	15	5	52	24	0
averages		inner i.d.	0	0	0	0	0	0	0	11	3	29	1	55
		outer i.d.	7	1	1	0	2	1	5	2	1	3	0	79
		base metal	0	2	2	1	0	0	0	15	5	53	21	0

[a] Results are normalized to 100 wt %. Points and areas are identified in the accompanying figures. Analysis by Microbeam Technologies, Inc. [b] Some or all of the reported sulfur may actually represent molybdenum.

Table 14. Corrosion of Reactor Interior Surface

	unaltered Hastelloy tubing		inner corrosion layer		outer corrosion layer
	manufacturer's specifications	PIXE[a,b]	SEMPC[a,c]	PIXE[a,b]	SEMPC[a,c]
Na	0.0	0.0	0.0	0.0	0.9
Mg	0.0	0.0	0.3	0.7	33.7
Al	0.0	0.4	0.3	0.4	5.8
Si	0.1[d]	0.1	0.3	0.4	12.2
P	0.0	0.0	0.0	0.6	0.0
S	0.0	0.0	0.0	0.0	0.0
Cl	0.0	0.0	0.0	0.0	2.7
K	0.0	0.0	0.0	0.0	13.7
Ca	0.0	0.0	0.3	0.7	23.5
V	0.4[d]	0.1	0.3	0.1	0.0
Cr	16.0	12.6	14.1	12.3	0.2
Mn	1.0[d]	0.8	0.5	0.8	0.0
Fe	5.0	5.6	4.3	5.6	6.4
Ni	57.0[e]	60.1	77.5	64.2	0.9
Mo	16.0	16.4	2.0	12.9	0.0
Co	2.5[d]	0.8	0.0	0.8	0.0
Cu	0.0	0.1	0.0	0.0	0.0
W	4.0	3.1	0.0	0.5	0.0

[a] PIXE values have been normalized to 100 wt % on a C-, H-, and O-free basis. SEMPC values have been normalized to 100 wt % on an O-free basis. (PIXE unaltered Hastelloy is 20.8% oxygen; PIXE corrosion layer is 11.1% H, 66.0% C, and 14.6% O; SEMPC inner corrosion layer is 55.0% O; and SEMPC outer corrosion layer is 60.4% O.) [b] The PIXE analysis was conducted by Elemental Analysis Corp. [c] SEM and SEMPC analyses were conducted by Microbeam Technologies, Inc. [d] Maximum. [e] As balance.

the reactions of interest. Under these circumstances, meaningful studies of the pathways, kinetics, and mechanisms of biomass gasification in supercritical water can conducted. Special attention should be given to the formation of tar during the pyrolysis of biomass in water and the catalytic gasification of tar by a packed bed of charcoal (or other carbons) in supercritical water.

Acknowledgment

This work was supported by NREL/DOE under cooperative agreement DE-FC36-94AL85804 and by the Coral Industries Endowment of the University of Hawaii at Manoa. We thank Neil Rosmeissl (DOE), Dr. Patrick Takahashi, and Dr. Richard Rocheleau (UH) for their interest and Mohammed Bayati (Barnebey and Sutcliffe Corp.) for the donation of the activated carbon used in this work. We also thank Jose Arteiro, Sonia Campbell, Tomas Ekbom, Patrick Girardot, Joe Lichwa, and Dr. Man Tam (UH) for assistance; Prof. Esteban Chornet (Sherbrooke University), Prof. Angela Garcia (University of Alicante), Dr. Johan Penninger (Twente University), Professor Galen Suppes (University of Kansas), Prof. Jefferson Tester (MIT) for useful advice; and two anonymous reviewers for their comments.

Literature Cited

(1) Antal, M. J. Tower Power: Producing Fuels from Solar Energy. In *Toward a Solar Civilization*; Williams, R. H., Ed.; MIT Press: Cambridge, MA, 1978; p 80.

(2) Antal, M. J. Synthesis Gas Production from Organic Wastes by Pyrolysis/Steam Reforming. In *Energy from Biomass and Wastes*; Klass, D. L., Ed.; IGT: Chicago, IL, 1978; pp 495−523.

(3) Van Hook, J. P. Methane-Steam Reforming. *Catal. Rev.−Sci. Eng.* **1980**, *21*, 1.

(4) Xu, J.; Froment, G. F. Methane Steam Reforming, Methanation and Water-Gas Shift: I. Intrinsic Kinetics. *AIChE J.* **1989**, *35*, 88.

(5) Xu, J.; Froment, G. F. Methane Steam Reforming: II. Diffusional Limitations and Reactor Simulation. *AIChE J.* **1989**, *35*, 97.

(6) Wagner, E. S.; Froment, G. F. Steam Reforming Analyzed. *Hydrocarbon Process.* **1992**, *July*, 69.

(7) Antal, M. J. Biomass Pyrolysis. Part 1: Carbohydrate Pyrolysis. In *Advances in Solar Energy*; Boer, K. W., Duffie, J. A., Eds.; Plenum Press: New York, 1982; p 61.

(8) Antal, M. J. The Effects of Reactor Severity on the Gas-Phase Pyrolysis of Cellulose and Kraft Lignin Derived Volatile Matter. *Ind. Eng. Chem. Res.* **1983**, *22*, 366.

(9) Antal, M. J. Biomass Pyrolysis. Part 2: Lignocellulose Pyrolysis. In *Advances in Solar Energy*; Boer, K. W., Duffie, J. A., Eds.; Plenum Press: New York, 1985; p 175.

(10) Antal, M. J. A Review of the Vapor Phase Pyrolysis of Biomass Derived Volatile Matter. In *Fundamentals of Thermochemical Biomass Conversion*; Overend, R. P., Milne, T. A., Mudge, L. K., Eds.; Elsevier Applied Science: New York, 1985; p 511.

(11) Herguido, J.; Corella, J.; Gonzalez-Saiz, J. Steam Gasification of Lignocellulosic Residues in a Fluidized Bed at a Small Pilot Scale. Effect of the Type of Feedstock. *Ind. Eng. Chem. Res.* **1992**, *31*, 1274.

(12) Delgado, J.; Aznar, M. P.; Corella, J. Biomass Gasification with Steam in Fluidized Bed: Effectiveness of CaO, MgO, and CaO−MgO for Hot Raw Gas Cleaning. *Ind. Eng. Chem. Res.* **1997**, *36*, 1535.

(13) Bridgwater, A. V. The Technical and Economic Feasibility of Biomass Gasification for Power Generation. *Fuel* **1995**, *74*, 631.

(14) Modell, M. Gasification and Liquefaction of Forest Products in Supercritical Water. In *Fundamentals of Thermochemical Biomass*; Overend, R. P., Milne, T. A., Eds.; Elsevier Applied Science Publishers: London, 1985; p 95.

(15) Antal, M. J.; Várhegyi, G. Cellulose Pyrolysis Kinetics: The Current State of Knowledge. *Ind. Eng. Chem. Res.* **1995**, *34*, 703.

(16) Antal, M. J.; Várhegyi, G.; Jakab, E. Cellulose Pyrolysis Kinetics: Revisited. *Ind. Eng. Chem. Res.* **1998**, *37*, 1267.

(17) Grønli, M.; Várhegyi, G.; Antal, M. J. A Round Robin Study of Cellulose Pyrolysis Kinetics by Thermogravimetry. *Ind. Eng. Chem. Res.* **1999**, *38*, 2238.

(18) Bobleter, O.; Binder, H. Dynamic Hydrothermal Degredation of Wood. *Holzforschung* **1980**, *34*, 48.

(19) Bouchard, J.; Nguyen, T. S.; Chornet, E.; Overend, R. P. Analytical Methods for Biomass Pretreatment. Part 1: Solid Residues. *Biomass* **1990**, *23*, 243.

(20) Bouchard, J.; Nguyen, T. S.; Chornet, E.; Overend, R. P. Analytical Methods for Biomass Pretreatment. Part 2: Characterization of the Filtrates and Cumulative Distribution as a Function of Treatment Severity. *Bioresour. Technol.* **1991**, *36*, 121.

(21) Mok, W. S. L.; Antal, M. J. Uncatalyzed Solvolysis of Whole Biomass Hemicellulose by Hot Compressed Liquid Water. *Ind. Eng. Chem. Res.* **1992**, *31*, 1157.

(22) Allen, S. G.; Antal, M. J.; Kam, L. C.; Zemann, A. J. Fractionation of Sugar Cane with Hot, Compressed, Liquid Water. *Ind. Eng. Chem. Res.* **1996**, *35*, 2709.

(23) Bobleter, O.; Concin, R. Degradation of Poplar Lignin by Hydrothermal Treatment. *Cell. Chem. Technol.* **1979**, *13*, 583.

(24) Antal, M. J.; Mok, W. S. L.; Richards, G. N. Mechanism of formation of 5-(hydroxymethyl)-2-furaldehyde from D-fructose and sucrose. *Carbohydr. Res.* **1990**, *199*, 91.

(25) Antal, M. J.; Mok, W. S. L.; Richards, G. N. Four-carbon model compounds for the reactions of sugars in water at high temperature. *Carbohydr. Res.* **1990**, *199*, 111.

(26) Antal, M. J.; Leesonboom, T.; Mok, W. S.; Richards, G. N. Mechanism of formation of 2-furaldehyde from D-xylose. *Carbohydr. Res.* **1991**, *217*, 71.

(27) Bobleter, O. Hydrothermal Degradation of Polymers Derived From Plants. *Prog. Polym. Sci.* **1994**, *19*, 797.

(28) Holgate, H. R.; Meyer, J. C.; Tester, W. J.; Glucose Hydrolysis and Oxidation in Supercritical Water. *AIChE J.* **1995**, *41*, 637.

(29) Kabyemela, B. M.; Takigawa, M.; Adschiri, T.; Malaluan, R. M.; Arai, K. Mechanism and Kinetics of Cellobiose Decomposition in Sub- and Supercritical Water. *Ind. Eng. Chem. Res.* **1998**, *37*, 357.

(30) Kabyemela, B. M.; Adschiri, T.; Malaluan, R. M.; Arai, K. Glucose and Fructose Decomposition in Subcritical and Supercritical Water: Detailed Reaction Pathway, Mechanisms, and Kinetics. *Ind. Eng. Chem. Res.* **1999**, *38*, 2888.

(31) Minowa, T.; Fang, Z.; Ogi, T.; Varhegyi, G. Decomposition of Cellulose and Glucose in Hot-Compressed Water under Catalyst-Free Conditions. *J. Chem. Eng. Jpn.* **1998**, *31*, 131. See also: Schmieder, H.; Abeln, J.; Boukis, N.; Dinjus, E.; Kruse, A.; Kluth, M.; Petrich, G.; Sadri, E.; Schacht, M. Hydrothermal Gasification of Biomass and Organic Wastes. *J. Supercrit. Fluids* **2000**, *17*, 145−153.

(32) Kabyemela, B. M.; Adschiri, T.; Malaluan, R.; Arai, K. Degradation Kinetics of Dihydroxyacetone and Glyceraldehyde in Subcritical and Supercritical Water. *Ind. Eng. Chem. Res.* **1997**, *36*, 2025.

(33) Kabyemela, B. M.; Adschiri, T.; Malaluan, R. M.; Arai, K. Kinetics of Glucose Epimerization and Decomposition in Subcritical and Supercritical Water. *Ind. Eng. Chem. Res.* **1997**, *36*, 1552.

(34) Boocock, D. G. B.; Sherman, K. M. Further Aspects of Powdered Poplar Wood Liquefaction by Aqueous Pyrolysis. *Can. J. Chem. Eng.* **1985**, *63*, 627.

(35) Jakab, E.; Liu, K.; Meuzelaar, H. L. C. Thermal Decomposition of Wood and Cellulose in the Presence of Solvent Vapors. *Ind. Eng. Chem. Res.* **1997**, *36*, 2087.

(36) Manarungson, S.; Mok, W. S. L.; Antal, M. J. Hydrogen Production by Steam Reforming Glucose in Supercritical Water. In *Advances in Thermochemical Biomass Conversion*; Bridgwater, A. V. Ed.; Blackie Academic & Professional: London, 1993; p 1367.

(37) Yu, D.; Aihara, M.; Antal, M. J., Jr. Hydrogen Production by Steam Reforming Glucose in Supercritical Water. *Energy Fuels* **1993**, *7*, 574.

(38) Xu, X.; Matsumura, Y.; Stenberg, J.; Antal, M. J. Carbon-Catalyzed Gasification of Organic Feedstocks in Supercritical Water. *Ind. Eng. Chem. Res.* **1996**, *35*, 2522.

(39) Corte, P.; Lacoste, C.; Traverse, J. P. Gasification and Catalytic Conversion of Biomass by Flash Pyrolysis. *J. Anal. Appl. Pyrolysis* **1985**, *7*, 323.

(40) Aznar, M. P.; Corella, J.; Delgado, J.; Lahoz, J. Improved Steam Gasification of Lignocellulosic Residues in a Fluidized Bed with Commercial Steam Reforming Catalysts. *Ind. Eng. Chem. Res.* **1993**, *32*, 1.

(41) Bridgwater, A. V. Catalysis in Thermal Biomass Conversion. *Appl. Catal. A: Gen.* **1994**, *116*, 5.

(42) Maggi, R.; Bernard, D. Characterization and Upgrading of Bio-oils Produced by Rapid Thermal Processing. *Biomass Bioenergy* **1994**, *7*, 245.

(43) Sealock, L. J., Jr.; Elliott, D. C.; Baker, E. G.; Fassbender, A. G.; Silva, L. J. Chemical Processing in High-Pressure Aqueous Environments. 5. New Processing Concepts. *Ind. Eng. Chem. Res.* **1996**, *35*, 411.

(44) Bangala, D. N.; Abatzoglou, N.; Martin, J.-P.; Chornet, E. Catalytic Gas Conditioning: Application to Biomass and Waste Gasification. *Ind. Eng. Chem. Res.* **1997**, *36*, 4184.

(45) Arauzo, J.; Radlein, D.; Piskorz, J.; Scott, D. S. Catalytic Pyrogasification of Biomass. Evaluation of Modified Nickel Catalysts. *Ind. Eng. Chem. Res.* **1997**, *36*, 67.

(46) Caballero, M. A.; Aznar, M. P.; Gil, J.; Martin, J. A.; Frances, E.; Corella, J. Commercial Steam Reforming Catalysts to Improve Biomass Gasification with Steam-Oxygen Mixtures. 1. Hot Gas Upgrading by the Catalytic Reactor. *Ind. Eng. Chem. Res.* **1997**, *36*, 5227.

(47) Narvaez, I.; Corella, J.; Orio, A. Fresh Tar (from a Biomass Gasifier) Elimination over a Commercial Steam-Reforming Catalyst. Kinetics and Effect of Different Variables of Operation. *Ind. Eng. Chem. Res.* **1997**, *36*, 317.

(48) Koningen, J.; Sjostrom, K. Sulfur-Deactivated Steam Reforming of Gasified Biomass. *Ind. Eng. Chem. Res.* **1998**, *37*, 341.

(49) Wang, D.; Czernik, S.; Chornet, E. Production of Hydrogen from Biomass by Catalytic Steam Reforming of Fast Pyrolysis Oils. *Energy Fuels* **1998**, *12*, 19.

(50) Aznar, M. P.; Caballero, M. A.; Gil, J.; Martin, J. A.; Corella, J. Commercial Steam Reforming Catalysts to Improve Biomass Gasification with Steam − Oxygen Mixtures. 2. Catalytic Tar Removal. *Ind. Eng. Chem. Res.* **1998**, *37*, 2668.

(51) Garcia, L.; Salvador, M. L.; Bilbao, R.; Arauzo, J. Influence of Calcination and Reduction Conditions on the Catalyst Performance in the Pyrolysis Process of Biomass. *Energy Fuels* **1998**, *12*, 139.

(52) Garcia, L.; Salvador, M. L.; Arauzo, J.; Bilbao, R. Influence of Catalyst Weight/Biomass Flow Rate Ratio on Gas Production in the Catalytic Pyrolysis of Pine Sawdust at Low Temperatures. *Ind. Eng. Chem. Res.* **1998**, *37*, 3812.

(53) Minowa, T.; Fang, Z. Hydrogen Production from Cellulose in Hot Compressed Water Using Reduced Nickel Catalyst: Production Distribution at Different Reaction Temperatures. *J. Chem. Eng. Jpn* **1998**, *31*, 488.

(54) Marquevich, M. C., S.; Chornet, E.; Montane, D. Hydrogen from Biomass: Steam Reforming of Model Compounds of Fast-Pyrolysis Oil. *Energy Fuels* **1999**, *13*, 1160.

(55) Gil, J. C., M. A.; Martin, J. A.; Aznar, M. P.; Corella, J. Biomass Gasification with Air in a Fluidized Bed: Effect of the In-Bed Use of Dolomite under Different Operation Conditions. *Ind. Eng. Chem. Res.* **1999**, *38*, 4226.

(56) Garcia, L.; Salvador, M. L.; Arauzo, J.; Bilbao, R. Catalytic Steam Gasification of Pine Sawdust. Effect of Catalyst Weight/Biomass Flow Rate and Steam/Biomass Ratios on Gas Production and Composition. *Energy Fuels* **1999**, *13*, 851.

(57) Minowa, T.; Ogi, T.; Yokoyama, S.-y. Hydrogen Production from Wet Cellulose by Low-Temperature Gasification Using a Reduced Nickel Catalyst. *Chem. Lett.* **1995**, 937.

(58) Kinoshita, C. M.; Wang, Y.; Zhou, J. Effect of Reformer Conditions on Catalytic Reforming of Biomass-Gasification Tars. *Ind. Eng. Chem. Res.* **1995,** *34*, 2949.

(59) Reed, T. B., Ed. *Biomass Gasification Principles and Technology*. Noyes Data Corp.: Park Ridge, NJ, 1981.

(60) Chern, S. M.; Walawender, W. P.; Fan, L. T. Mass and Energy Balance Analysis of a Downdraft Gasifier. *Biomass* **1989**, *18*, 127.

(61) Cookson, J. T., Jr. Physicochemical Changes of Substances by or within Carbon Adsorption Beds. In *Activated Carbon Adsorption of Organics from the Aqueous Phase*; Suffet, I. H., McGuire, M. J., Eds.; Ann Arbor Science Publishers: Ann Arbor, MI, 1980; p 379.

(62) Radovic, L. R.; Sudhakar, C. Carbon as a Catalyst Support: Production, Properties and Applications. In *Introduction to Carbon Technologies*; Marsh, H., Heintz, E. A., Rodriguez-Reinoso, F., Eds.; Universidad de Alicante: Alicante, Spain, 1997; p 103.

(63) Matsumura, Y.; Xu, X.; Antal, M. J. Gasification Characteristics of an Activated Carbon in Supercritical Water. *Carbon* **1997**, *35*, 819.

(64) Matsumura, Y.; Adschiri, T.; Xu, X.; Garcia, A.; Antal, M. J., Jr. Reaction Rate of Activated Carbon with Supercritical Water. The 4th Interntational Symposium on Supercritical Fluids, Sendai, Japan, 1997; p 555.

Received for review March 20, 2000
Revised manuscript received July 11, 2000
Accepted August 10, 2000

IE0003436